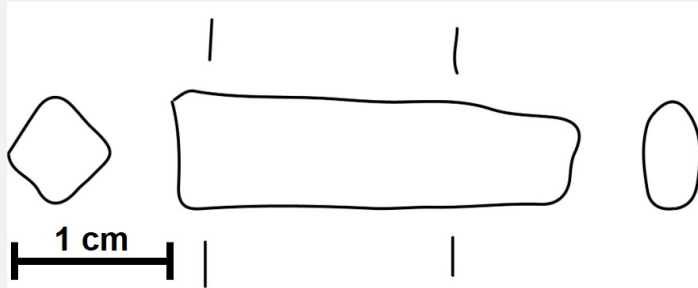


TANG FRAGMENT OF A KNIFE HR-6246 – TIN BRONZE – LATE BRONZE AGE – SWITZERLAND

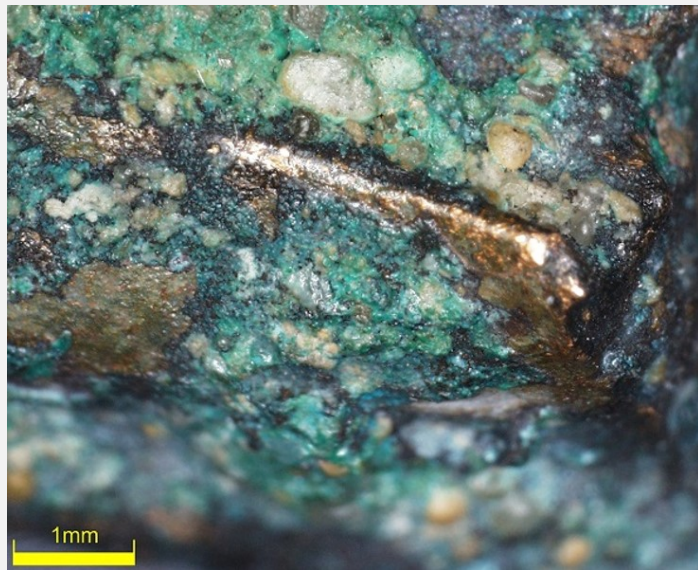
Artefact name	Tang fragment of a knife HR-6246
Authors	Marianne. Senn (Empa, Dübendorf, Zurich, Switzerland) & Christian. Degrigny (HE-Arc CR, Neuchâtel, Neuchâtel, Switzerland) & Naima. Gutknecht (HE-Arc CR, Neuchâtel, Neuchâtel, Switzerland) & Rémy. Léopold (HE-Arc CR, Neuchâtel, Neuchâtel, Switzerland)
Url	/artefacts/1038/

∨ The object



Credit Laténium.

Fig. 1: Tang fragment of a knife (after Rychner-Faraggi 1983, plate 35.35),



Credit HE-Arc CR, N.Gutknecht.

Fig. 2: Shiny yellow and green-blue corrosion products on the surface of the tang fragment of a knife,

∨ Description and visual observation

Description of the artefact	Tang fragment of a knife with shiny yellow and green-blue corrosion products (Figs. 1 & 2). Dimensions: L = 2.7cm; Ø = around 5mm; WT = 5.8g.
Type of artefact	Household implement
Origin	Hauterive - Champréveyres, Neuchâtel, Neuchâtel, Switzerland
Recovering date	Excavation 1983-1985, object from layer 1 (layer with material from Bronze Age till 20th cent.)
Chronology category	Late Bronze Age
chronology tpq	<input type="text" value="1050"/> B.C. ▾
chronology taq	<input type="text" value="800"/> B.C. ▾
Chronology comment	Hallstatt A/B

Burial conditions / environment	Lake
Artefact location	Laténium, Neuchâtel, Neuchâtel
Owner	Laténium, Neuchâtel, Neuchâtel
Inv. number	Hr 6246
Recorded conservation data	N/A

Complementary information

The object was sampled in 1987 for analysis. Documentation of the strata in binocular mode on the remaining fragment of the object was performed in 2022.

Study area(s)

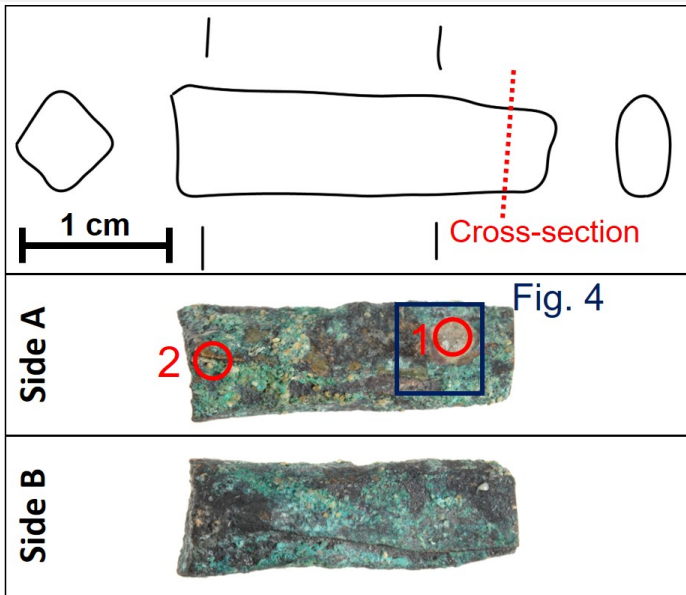


Fig. 3: Location of the cross-section before sampling and both sides of the fragment not sampled with location of the detail of Fig. 4 (blue square) and XRF analysis areas (red circles),

Credit HE-Arc CR, N. Gutknecht.

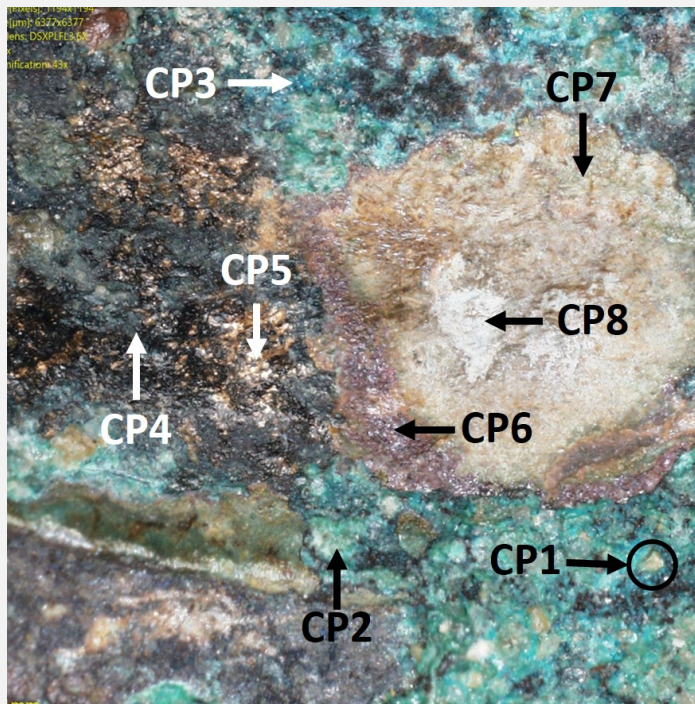


Fig. 4: Corrosion structure (detail) from Fig. 3 showing some of the documented strata,

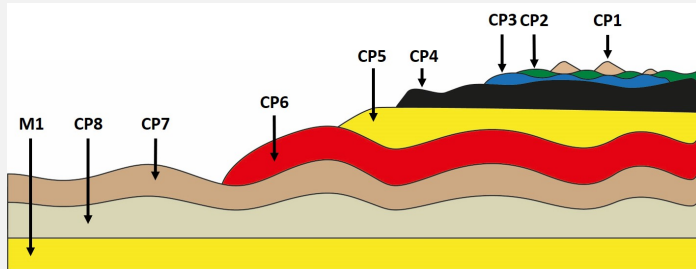
Credit HE-Arc CR, N. Gutknecht.

Binocular observation and representation of the corrosion structure

The schematic representation below gives an overview of the corrosion structure encountered on the tang from a first visual macroscopic observation.

Strata	Type of stratum	Principal characteristics
CP1	Corrosion product	Nodule, light brown, thin, scattered, compact, severable, very soft
CP2	Corrosion product	Dark green, submetallic, thin, scattered, compact, tough, soft
CP3	Corrosion product	Blue, submetallic, thin, scattered, compact, tough, soft
CP4	Corrosion product	Black, resinous, thin, discontinuous, compact, malleable, very soft
CP5	Corrosion product	Yellow, metallic, medium (thickness), discontinuous, compact, brittle, hard
CP6	Corrosion product	Red, adamantine, thin, continuous, non-compact, friable, soft
CP7	Corrosion product	Light brown, matte, thin, continuous, compact, friable, soft
CP8	Corrosion product	Light yellow, matte, thin, continuous, non-compact, powdery, very soft
M1	Metal	Yellow, thick, metallic, soft

Table 1: Description of the principal characteristics of the strata as observed under binocular and described according to Bertholon's method.



Credit HE-Arc CR, N.Gutknecht.

Fig. 5: Stratigraphic representation of the corrosion structure of the tang by macroscopic and binocular observation with reference to Fig. 4,

✓ MiCorr stratigraphy(ies) – Bi

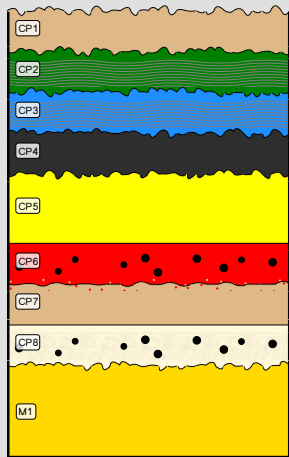
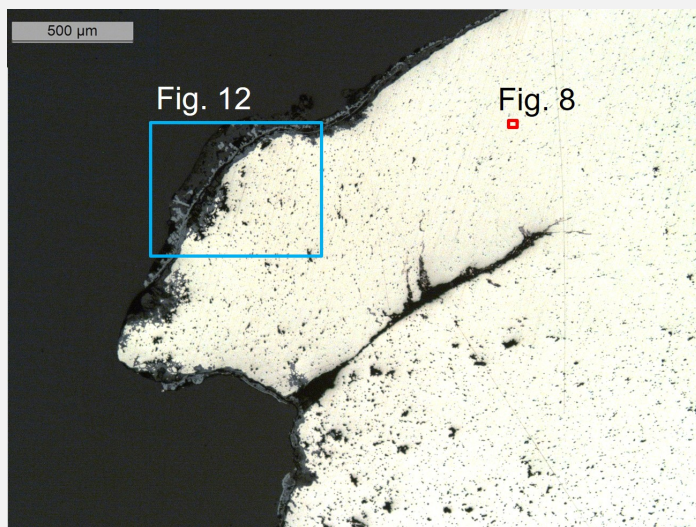


Fig. 6: Stratigraphic representation of the corrosion structure of the tang observed macroscopically under binocular microscope using the MiCorr application with reference to the whole Fig. 5. The characteristics of the strata, such as discontinuity, are accessible by clicking on the drawing that redirects you to the search tool by stratigraphy representation, Credit HE-Arc CR, N.Gutknecht,

✓ Sample(s)



Credit HE-Arc CR, L.Rémy.

Fig. 7: Micrograph from an area of the cross-section of the sample taken from the tang fragment with location of Fig. 8 (red square) and Fig. 12 (blue square), unetched, bright field,

Description of sample	The cross-section corresponds to a lateral cut (Fig. 3). The surface is covered with a thick corrosion layer but part of it has gone (Fig. 7).
Alloy	Tin Bronze
Technology	Cold worked with partial annealing
Lab number of sample	MAH 87-197
Sample location	Musées d'art et d'histoire, Genève, Geneva
Responsible institution	Musées d'art et d'histoire, Genève, Geneva
Date and aim of sampling	1987, metallography and corrosion characterisation

Complementary information

This sample is mentioned in Schweizer, 1994.

Analyses and results

Analyses performed:

Non-invasive approach

XRF with handheld portable X-ray fluorescence spectrometer (NITON XL5). General Metal mode, acquisition time 60s (filters: Li20/Lo20/M20).

Invasive approach (on the sample)

Metallography (etched with ferric chloride reagent), Vickers hardness testing, ICP-OES (conditions provided in the About tab of the MiCorr application), SEM/EDS (20keV, Microcity), XRD.

Non invasive analysis

XRF analyses of the tang fragment were carried out on two representative areas (Fig. 3). Point 1 was done in a lacuna of the green-blue corrosion layer, while point 2 was performed on a black corrosion layer (CP4) where all strata (soil, corrosion products, and metal) are analyzed at the same time.

The metal is presumably a tin bronze alloy. The other elements detected are : S, Si, Pb, Sb, Fe, As, Ni, Ag, Zn, Co.

Both results are similar.

Elements (mass %)	Cu		Sn		S		Si		Pb		Sb		Fe		As		Ni		Ag		Zn		Co		Total
	%	+/- 2σ	%	+/- 2σ	%	+/- 2σ	%	+/- 2σ	%	+/- 2σ	%	+/- 2σ	%	+/- 2σ	%	+/- 2σ	%	+/- 2σ	%	+/- 2σ	%	+/- 2σ	%	+/- 2σ	
1	83.0	0.1	10.0	0.05	2.5	0.03	1.5	0.05	0.5	0.02	0.5	0.02	0.4	0.02	0.4	0.03	0.3	0.01	0.2	0.01	0.1	0.02	<0.1	0.01	99.4
2	81.0	0.2	9.0	0.06	2.0	0.04	0.7	0.09	0.7	0.02	0.7	0.02	0.5	0.02	1.0	0.03	0.3	0.02	0.3	0.01	0.1	0.03	<0.1	0.01	99.3

Table 2: Chemical composition of the surface of the tang at two representative areas shown in Fig. 3. Method of analysis: XRF.

Metal

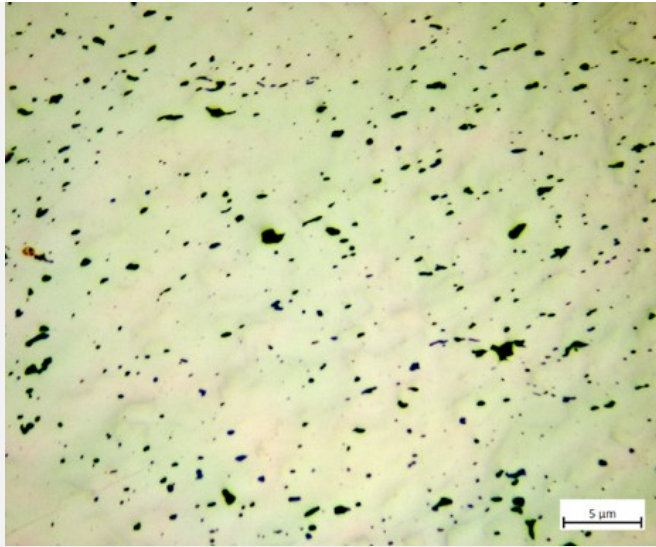
The remaining metal is a tin bronze (Table 3) with high porosity (Figs. 7-9) and large cracks both on the left and right edges of the sample (Fig. 9). The metal contains small, elongated copper sulphide (Table 4) and Pb inclusions. The etched metal shows three zones with a core where elongated grains and slip lines are visible indicating cold working without annealing (Figs. 9-10), while annealing appears on both external sides (Fig. 9-11). The average hardness of the metal is HV1 145, but significant variations are observed, depending on where the measurements are taken.

Elements	Cu	Sn	Sb	Ni	Pb	As	Ag	Co	Fe	Zn
mass%	89.85	8.02	0.60	0.55	0.34	0.34	0.18	0.10	0.02	0.01

Table 3: Chemical composition of the metal. Method of analysis: ICP-OES, Laboratory of Analytical Chemistry, Empa.

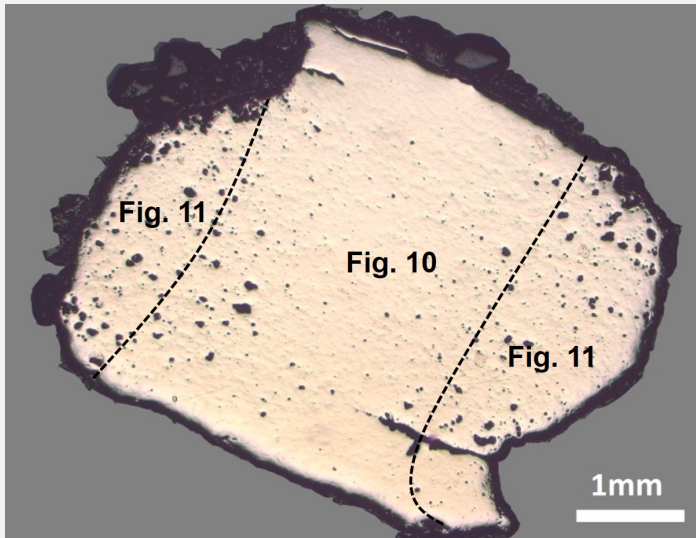
Elements	O	S	Cu	Total
mass%	0.9	20	77	98

Table 4: Chemical composition of inclusions. Method of analysis: SEM/EDS, Laboratory of Analytical Chemistry, Empa.



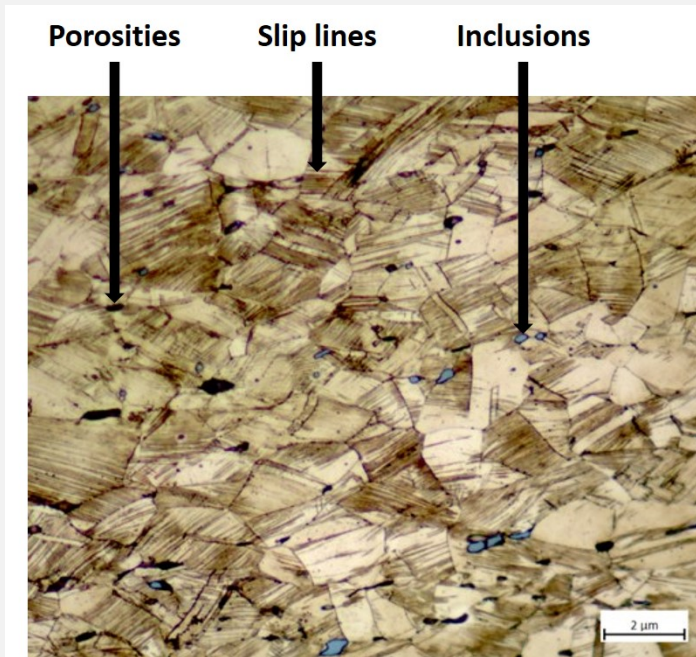
Credit HE-Arc CR, L.Rémy.

Fig. 8: Detail of the metal from Fig. 7, unetched, bright field,



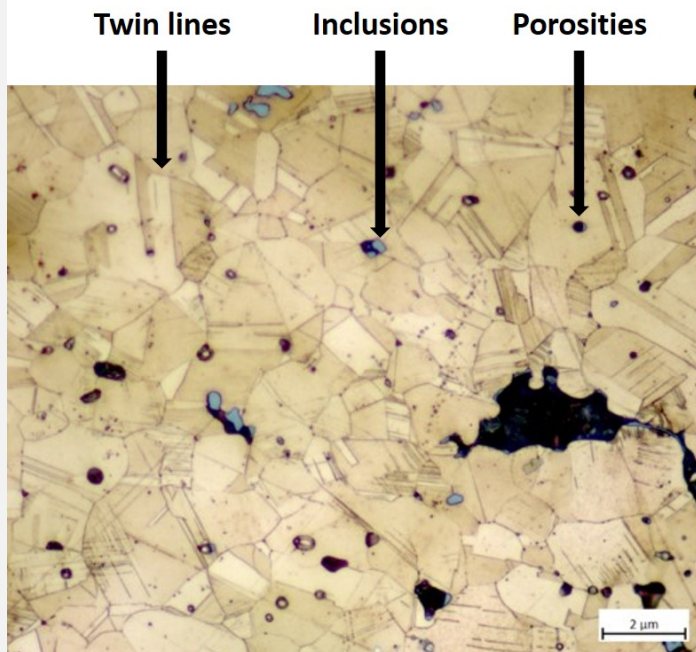
Credit HE-Arc CR, L.Rémy.

Fig. 9: Micrograph of the cross section of the tang of a knife with three distinct zones: metal core with elongated grains and slip lines (Fig. 10) and external sides with polygonal grains and twin lines (Fig. 11), unetched, bright field,



Credit HE-Arc CR, L.Rémy.

Fig. 10: Micrograph of the metal sample from Fig. 9 (detail), etched, bright field. Elongated grains with slip lines are observed, as well as grey copper sulphide inclusions and dark porosities,



Credit HE-Arc CR, L.Rémy.

Fig. 11: Micrograph of the metal sample from Fig. 9 (detail), etched, bright field. Twin lines, grey copper sulphide inclusions and dark porosity are observed,

Microstructure	Mixture of elongated grains with slip lines and polygonal grains with twin lines
First metal element	Cu
Other metal elements	Co, Ni, As, Ag, Sn, Sb, Pb

Complementary information

Schweizer (1994) indicates that the copper-tin alloys similar to the one of the tang have minor constituents that were certainly not added intentionally. Furthermore, he mentions that there is no systematic composition difference between bronzes with a lake patina and those with a land patina.

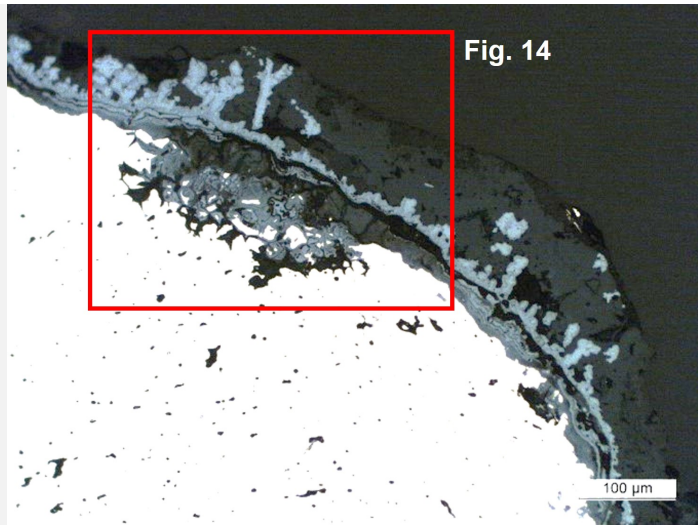
Corrosion layers

The corrosion layer has a thickness between 130μm and 70μm (Fig. 12). The observation of the sample in cross-section (Figs. 12-13) shows the presence of a succession of layers : S1 sediment, at the very top surface; CP1 thick continuous layer, dark grey in bright field, dark turquoise in dark field; CP2 thin continuous layer which might expand through the whole CP1, extra light grey in bright field, black in dark field; CP3 thin continuous layer, extra light grey in bright field, light brown in dark field; CP4 medium discontinuous layer, dark grey in bright field, light green in dark field; CP5 medium continuous layer, light grey in bright field, dark orange in dark field; CP6 thin discontinuous layer, black in bright field, light brown in dark field; CM1 medium discontinuous layer;

The elemental chemical distribution (Fig. 15) of the SEM image (Fig. 14) of the visually identified strata by cross-sectional observation shows that :

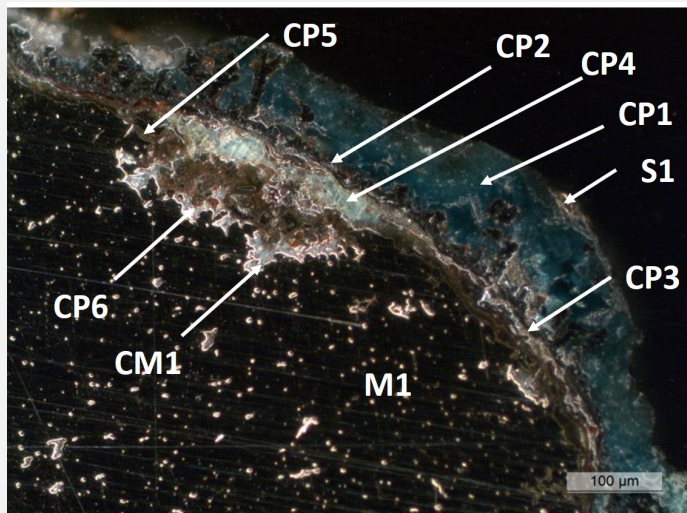
- S1 has Ca, Al, Si and O elements;
- CP1 stratum contains Cu, O and S;
- CP2 stratum contains Cu, S and Fe;
- CP3 stratum contains Sn, Fe and S;
- CP4 stratum contains Sn and O;
- CP5 stratum contains Cu, O and S;
- CP6 stratum contains Sn and O, similar to CP4;

XRD analyses indicated the presence of posnjakite/Cu₄SO₄(OH)₆H₂O, chalcocite/Cu₂S and djurleite/Cu_{1.93}S (Schweizer 1994).



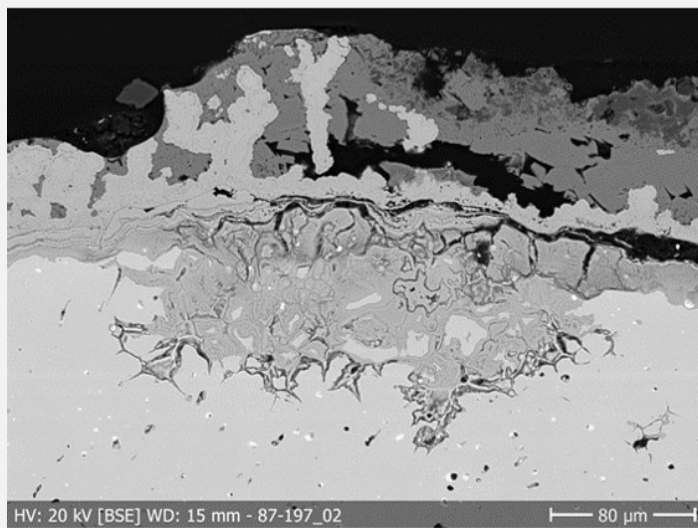
Credit HE-Arc CR, L.Rémy.

Fig. 12: Micrograph of the metal sample from Fig. 7 (detail, rotated of 90°), unetched, bright field.



Credit HE-Arc CR, L.Rémy.

Fig. 13: Micrograph similar to Fig. 12, unetched, dark field and corresponding to the stratigraphy of Fig. 16,



Credit HE-Arc CR, S.Ramseyer.

Fig. 14: SEM image, BSE-mode (detail of Fig. 12),

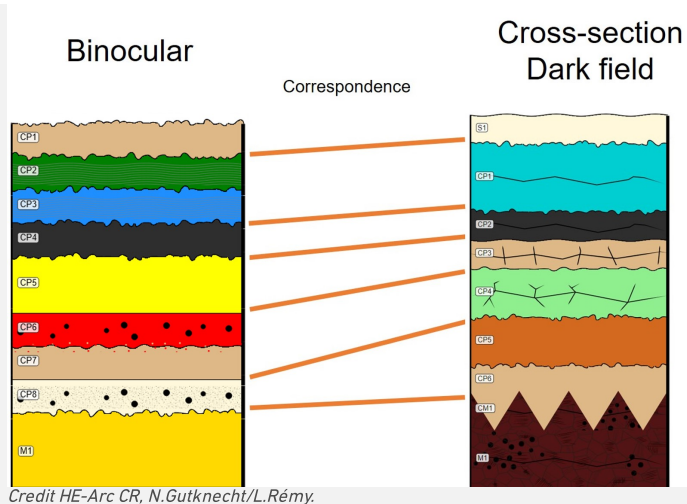


Fig. 17: Stratigraphic representation side by side of binocular view and cross-section (dark field),

Credit HE-Arc CR, N.Gutknecht/L.Rémy.

Conclusion

The tang fragment is made from a tin bronze and has been cold worked with partial annealing since slip lines are still visible. Past XRD analyses indicate the presence of chalcopyrite in the corrosion layer, typical of lake context (Schweizer 1994), which we seem to have found locally in the corrosion structure. This object was certainly abandoned rather quickly in an anaerobic, humid and S and Fe-rich environment, favouring then the formation of chalcopyrite, before being exposed in an aerated environment in which the corrosion structure was formed. The limit of the original surface most probably lies between the Sn-rich inner layer and the Fe/Cu and S-rich outer layers. The corrosion is a type 1 according Robbiola et al. 1998.

This object was first sampled in 1987. Thanks to an extensive documentation on the cross-section and comparison with similar objects (see references), Schweizer defines a "land patina" typology on this object.

References

References on object and sample

Object files in MiCorr

1. MiCorr_Pin or needle fragment HR-3031
2. MiCorr_Tang fragment of a knife HR-6567
3. MiCorr_Pin HR-17773
4. MiCorr_Pin HR-3071
5. MiCorr_Pin HR-18603
6. MiCorr_Pin HR-3389
7. MiCorr_Pin HR-18152

References object

8. Rychner-Faraggi A-M. (1993) Hauterive – Champréveyres 9. Métal et parure au Bronze final. Archéologie neuchâteloise, 17 (Neuchâtel).

References sample

9. Rapport d'examen, Laboratoire Musées d'art et d'histoire, Geneva GE (1987), 87-194 à 197.
10. Schwartz, G.M. (1934) Paragenesis of oxidised ores of copper, Economic Geology, 29, 55-75.
11. Schweizer, F. (1994) Bronze objects from Lake sites: from patina to bibliography. In: Ancient and historic metals, conservation and scientific research (eds. Scott, D.A., Podany, J. and Considine B.B.), The Getty Conservation Institute, 33-50.

References on analytic methods and interpretation

12. Robbiola, L., Blengino, J-M., Fiaud, C. (1998) Morphology and mechanisms of formation of natural patinas on archaeological Cu-Sn alloys, Corrosion Science, 40, 12, 2083-2111.